ANZIAM J. **67, e28** (2025), 1–32
doi:10.1017/S1446181125100114

RESONANT DYNAMIC B-TIPPING CLOSE TO A NONSMOOTH SADDLE-FOCUS BIFURCATION LINKED TO CLIMATE CHANGE

CHRISTOPHER BUDD[1] and RACHEL KUSKE[2]

(Received 7 October, 2024; accepted 9 April, 2025)

Abstract

We study the behaviour of (resonant) dynamic B-tipping in a forced two-dimensional nonautonomous system, close to a nonsmooth saddle-focus (NSF) bifurcation. The NSF arises when a saddle-point and a focus meet at a border collision bifurcation. The emphasis is on the Stommel 2-box model, which is a piecewise-smooth continuous dynamical system, modelling thermohaline circulation. This model exhibits an NSF as parameters vary. By using techniques from the theory of nonsmooth dynamical systems, we are able to provide precise estimates for the general tipping behaviour close to the bifurcation as parameters vary. In particular, we consider the combination of both slow drift and also periodic changes in the parameters, corresponding, for example, to the effects of slow climate change and seasonal variations. The results are significantly different from the usual B-tipping point estimates close to a saddle-node bifurcation. In particular, we see a more rapid rate of tipping in the slow drift case, and an advancing of the tipping point under periodic changes. The latter is made much more pronounced when the periodic variation resonates with the natural frequency of the focus, leading both to much more complicated behaviour close to tipping and also significantly advanced tipping in this case.

2020 *Mathematics subject classification*: primary 37G15; secondary 37G35, 37N10.
Keywords and phrases: tipping points, saddle-focus bifurcation, Stommel box model.

1. Introduction

1.1. Overview Various models of phenomena in climate have been used both to model and to predict abrupt changes in systems with a wide range of time scales. As a result, there are many climate models that include nonsmooth features

[1]Department of Mathematics, University of Bath, Bath BA2 7AY, UK; e-mail: mascjb@bath.ac.uk
[2]School of Mathematics, Georgia Institute of Technology, Atlanta, GA, USA;
e-mail: rkuske7@gatech.edu

approximating transitions over short times relative to climate time scales. These include state-dependent switches, nonsmooth functional descriptions of dynamics and discrete states delineated by boundaries. Examples of these are given by the PP04 model of sudden changes in carbon dioxide emission rates during glacial cycles [16, 17], rainfall [11], the motion of the ice fronts in a glacial cycle [24], as well as the Stommel 2-box model for thermohaline circulation that we study in this paper. In all such systems, we see both the dynamics commonly found in smooth systems (such as possibly co-existing periodic and chaotic states and transitions between them including tipping points), as well as dynamical behaviours specific to nonsmooth systems, such as grazing, sliding and nonsmooth bifurcations between different co-existing states [4].

Transitions in the context of bi-stability have been studied in many contexts. A common setting is where stability is lost at bifurcation points, and the system experiences hysteresis as parameters vary through these points, depending upon the form of the parameter variation. For these nonautonomous systems with varying parameters, the transitions between states may be qualitatively different, depending on the nonlinearities, the types of underlying static bifurcations and the vector fields near the stable equilibria. Throughout this paper, we use the term *B-tipping* to refer to a sudden transition from one qualitatively different state to another in the nonautonomous setting, close to a static bifurcation. More broadly, the term tipping is used in a wider variety of settings, see for example [1], to describe a qualitative change in behaviour along a particular time-varying trajectory. Bifurcations and tipping are often related, as tipping may be related to a bifurcation point or some other separatrix of a particular object in the flow, such as a fold point of a slow manifold or stable manifold of a saddle. This relationship is indeed present in the systems we study here: the nonautonomous systems with time-varying parameters have autonomous counterparts with static parameters treated as bifurcation parameters. Given this connection, we use the term dynamic bifurcation to refer to the specific setting where a parameter value varies in time near or through the critical value of a static bifurcation parameter from an underlying autonomous system.

In this paper, we focus on the dynamic transitions near to a *nonsmooth saddle-focus* (NSF) bifurcation in a parametrized, forced, nonsmooth two-dimensional (2D) system (a reduction of the Stommel 2-box model). The NSF arises when a focus (F) and a saddle point (S) coalesce at a border collision bifurcation (BCB) when a parameter μ is varied. We consider the dynamic transitions, in particular tipping phenomenon, as the parameter μ is slowly varied through this bifurcation, combined with a periodic forcing of the system. We obtain results that can be contrasted with analogous transitions near smooth saddle-node bifurcations (SNBs) [26]. In an earlier paper [6], we considered B-tipping close to a nonsmooth saddle-node bifurcation in a one-dimensional (1D) problem where a stable and an unstable node coalesce, also at a BCB. Estimates were obtained of the location of the tipping point in the case of a dynamic parameter that had both a slow drift and an oscillatory variation. The 2D case considered in this paper is more realistic as a climate model than the 1D problem. Whilst similar to the

https://doi.org/10.1017/S1446181125100114 Published online by Cambridge University Press

1D problem (in particular, for the case of high-frequency forcing), the 2D case also has a richer dynamics, particularly when the frequency of the forcing resonates with the natural frequency of the focus. In this paper, we obtain expressions for the tipping point with and without parameter drift in this nonsmooth model in the cases of rapid forcing, slow forcing and resonant forcing. Specifically, we show that tipping occurs earlier, more abruptly and in a less predictable manner, closer to an (nonsmooth) NSF than in the case of tipping at a (smooth) SNB. This tipping is further advanced by the impact of resonance of the periodic forcing with the natural frequency of the focus. We compare our conclusions to observed phenomena in climate dynamics through a comparison with the Stommel 2-box climate model. In particular, we find conditions for sudden transitions between temperature-dominated and salinity-dominated states. In a further study, we will look at the impact of noise on the location of tipping points close to an NSF, showing that it also tends to advance the location of tipping points.

1.2. Results We study the dynamics of the (nonsmooth) Stommel 2-box model of the Atlantic meridional overturning circulation (AMOC) [7] close to an NSF. In particular, we investigate a periodically (seasonally) forced, parametrized piece-wise linear system which is a reduction of the full model close to the coalescence of a saddle and a focus at a border collision bifurcation. The NSF occurs when the bifurcation parameter μ reduces to $\mu = 0$. If μ has a slow drift through zero of rate $\epsilon \ll 1$ and the periodic forcing is given by $A\sin(\omega t)$, then we see B-tipping behaviour close to the NSF. The form of this differs in many respects from both B-tipping with drift at an SNB [10] and also the oscillatory forced tipping seen at the 1D nonsmooth fold considered in [6]. The main conclusion of this work is that the impact of resonance between the natural frequency of the focus at the NSF and the frequency ω of the forcing is to significantly advance tipping. More particularly, we have the following results.

(1) For the case of slow drift through the NSF without periodic forcing ($A = 0$), B-tipping in the Stommel 2-box model is very similar to the 1D model in [6]. If the drift rate is ϵ, then (to leading order) B-tipping occurs when the bifurcation parameter $\mu \sim -C_1\epsilon\log(K/\epsilon)$, $C_1 > 0$.
(2) If the system has periodic forcing and no parameter drift ($\epsilon = 0$), so that the parameter μ is fixed, then for larger values of μ, there is always a stable periodic orbit. This orbit loses stability as μ decreases and we see tipping.
    (a) For high-frequency forcing of frequency $\omega \gg 1$, B-tipping occurs from a stable periodic orbit at a cyclic-fold bifurcation point μ_c. This tipping point can be estimated with high accuracy to be $\mu_c \sim C_2/\omega$, where $C_2 > 0$ is given analytically. Close to tipping, the stable periodic orbit takes on a figure-of-eight form.
    (b) If the forcing has a low frequency$\omega \ll 1$ with scaled amplitude$A = 1$, we see tipping from the stable periodic orbit at the parameter value $\mu_c \sim 1 + C_3\omega^2$, $C_3 > 0$. In this case, the periodic orbit has an "L-shaped" form.

https://doi.org/10.1017/S1446181125100114 Published online by Cambridge University Press

(c) If the forcing frequency $\omega \approx 1$ is close to the natural frequency of the focus, then the system is near resonant with complex (sometimes chaotic) periodic orbits arising at period doubling bifurcations as μ deceases. The impact of resonance is to increase the value of the tipping point μ_c and to advance tipping.

(3) If the system is both periodically forced and the parameter μ has nonzero drift, then the value of the tipping point μ is (apart from the high-frequency limit) a complex and nonmonotonic function of both the drift rate ϵ and the forcing frequency ω. In all cases, *tipping is significantly advanced* when ω is close to the resonant values.

1.3. Summary The remainder of this paper is structured as follows. In Section 2, we describe the forced Stommel 2-box model, and identify its (smooth and nonsmooth) bifurcation points (including the NSF) and related tipping dynamics. In Section 3, we derive a normal form for the dynamics of a forced system close to the NSF and determine simple properties of its dynamics. In Section 4, we give estimates for B-tipping when the system has slow drift. In Section 5, we study the system under high-frequency forcing with no drift and give asymptotic estimates for the tipping point. In Section 6, we repeat this analysis for low-frequency forcing and in Section 7, for near-resonant forcing showing the existence of complex orbits and advanced tipping in this case. In Section 8, we consider tipping under the combination of slow drift and periodic forcing, showing that the tipping point is very sensitively dependent on the system parameters. In Section 9, we discuss the climatic implications of these results. Finally, in Section 10, we draw some conclusions from this work.

2. Overview of AMOC and the Stommel 2-box model

2.1. The Stommel 2-box model A well-known class of climate models, where salinity-dominated and temperature-dominated states are bi-stable, is that of thermohaline circulation (THC). Here, abrupt qualitative changes are possible, see Alley et al. [2], Marotzke [15] or Rahmstorf [18, 19]. Recently, Rahmstorf was able to find evidence of weakening occurring around these abrupt changes in the AMOC system of ocean patterns [7]. This evidence of ocean dynamics responding to changes in surface temperature underscores the need to understand the transitions in these types of systems. We note that such transitions can be either smooth or nonsmooth (as described in [4]). In this paper, we focus on the commonly used Stommel 2-box model [23] as an exemplar for studying the transitions in the THC (or more generally, the dynamical impact of NSF bifurcations between equilibrium states) in a realistic climate model. We begin with the nondimensionalized Stommel 2-box model as given in [8]:

$$\begin{aligned} \dot{\mathcal{T}} &= \eta_1 - \mathcal{T}(1 + |\mathcal{T} - \mathcal{S}|), \\ \dot{\mathcal{S}} &= \eta_2 - \mathcal{S}(\eta_3 + |\mathcal{T} - \mathcal{S}|). \end{aligned} \tag{2.1}$$

https://doi.org/10.1017/S1446181125100114 Published online by Cambridge University Press

Here, the variables $\mathcal{T}$ and $\mathcal{S}$ are the dimensionless equatorial-to-pole differences for temperature and salinity, respectively. The parameters η_1, η_2 and η_3 are also dimensionless quantities, with η_1 representing thermal variation, η_2 is the freshwater flux, and η_3 is the ratio of relaxation times of temperature and salinity. The dimensionless AMOC strength is captured by the difference

$$\mathcal{V} = \mathcal{T} - \mathcal{S},$$

which plays an important role throughout the dynamical analysis. We can then express this system as

$$\begin{aligned} \dot{\mathcal{T}} &= \eta_1 - \mathcal{T}(1 + |\mathcal{V}|), \\ \dot{\mathcal{V}} &= \eta_1 - \eta_2 + \eta_3(\mathcal{T} - \mathcal{V}) - \mathcal{T} - \mathcal{V}|\mathcal{V}|. \end{aligned} \tag{2.2}$$

With the dependence on the absolute value $|\mathcal{V}|$, (2.2) is a *nonsmooth dynamical system*. It has a *discontinuity surface* Σ given by

$$\Sigma = \{\mathcal{V} = 0\},$$

across which we see a discontinuity in $d^2\mathcal{T}/dt^2$ and $d^2\mathcal{V}/dt^2$. The equations for $\mathcal{T}$ and $\mathcal{V}$ then describe different dynamics in Σ^+ (the temperature-dominated state) and Σ^- (the salinity-dominated state) for

$$\Sigma^+ = \{(\mathcal{T}, \mathcal{V}) \mid \mathcal{V} > 0\}, \quad \Sigma^- = \{(\mathcal{T}, \mathcal{V}) \mid \mathcal{V} < 0\}.$$

The model is nonsmooth through the action of the nonlinearity $|\mathcal{T} - \mathcal{S}|$ and takes the form of a *piecewise-smooth continuous system* with a degree of discontinuity equal to 2 [4, 22].

2.2. Static dynamics It is straightforward to analyse the Stommel 2-box model in the case of static parameters η_i [8, 12]. A standard analysis of the static model, where typically η_1 and η_3 are fixed, and η_2 is treated as a bifurcation parameter, yields stability regions for the temperature and salinity-dominated states. Taking values of η_1 and η_3 (typically $\eta_1 = 3, \eta_3 = 0.3$) as is usual in applications [8], there are either three or one fixed points. In the case of three fixed points, we identify two different critical bifurcation points, denoted as η_{2sn} and $\eta_{2sf} = \eta_1\eta_3$, with $\eta_{2sn} > \eta_{2sf}$.

For $\eta_{2sn} > \eta_2 > \eta_{2sf}$, there are two fixed points in Σ^+ which are respectively a saddle (**S**) and a stable node (**N**). The saddle and node coalesce at the (smooth) SNB η_{2sn} and cease to exist for $\eta_2 > \eta_{2sn}$.

For $\eta_2 > \eta_{2sf}$, there is a further fixed point in Σ^-, which is a stable *focus* (**F**). If $\eta_2 < \eta_{2sf}$, there is only the stable node **N** in Σ^+. These observations are illustrated in Figure 1 for $\mathcal{V}$ versus η_2. Note that **N** corresponds to the temperature-dominated state with $\mathcal{T} > \mathcal{S}$, and **F** corresponds to the salinity-dominated state with $\mathcal{S} > \mathcal{T}$.

The critical point η_{2sf}, indicated by an o in Figure 1, arises at a BCB [4]. This occurs when **F** and **S** intersect with Σ. This critical point can be obtained from (2.1) as

$$\eta_{2sf} \equiv \eta_1\eta_3.$$

https://doi.org/10.1017/S1446181125100114 Published online by Cambridge University Press

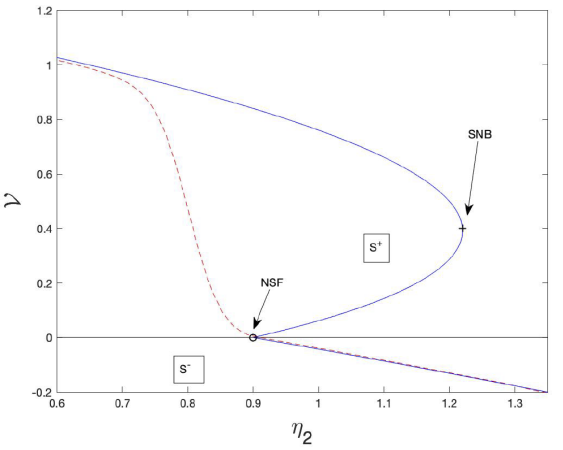

FIGURE 1. The static bifurcation diagram for the Stommel 2-box model showing $\mathcal{V}$ as a function of η_2 (blue) when $\eta_1 = 3, \eta_3 = 0.3$. The saddle-focus (NSF) at $\eta_{2sf} = \eta_1\eta_3$ is indicated by an o, and the saddle node (SNB) by a +. Tipping at the NSF due to drift when $\eta_2 = 1.35 - 0.025\, t$ is shown in dashed red. We also show the regions S^+ and S^-, and the discontinuity set Σ at $\mathcal{V} = 0$.

This (NSF) bifurcation is a nonsmooth fold [4], in which **F** and **S** co-exist if $\eta_2 > \eta_{2sf}$ and neither exist if $\eta_2 < \eta_{2sf}$. Close to η_{2sf}, the NSF has a V-shaped form, with the focus and saddle point having the form of $(\mathcal{T}^{\pm}, \mathcal{V}^{\pm})$ with $\mathcal{V}^{\pm}$ proportional to $\pm\mu$, where $\mu = \eta_2 - \eta_{2sf}$.

The coalescence of a saddle **S** with a focus **F** can only occur, because this is a nonsmooth system. Such bifurcations do not arise in smooth systems where an SNB necessarily indicates collision of a stable node and a saddle. The mathematical structure near $(\eta_{2sf}, 0)$ (indicated by an o in Figure 1) is substantially different from that near the smooth SNB $(\eta_{sn}, \mathcal{V}_{2sn})$ (indicated by a + in Figure 1). In particular, at the saddle-focus NSF, the real parts of the eigenvalues of the linearizations of either of the fixed points (saddle and focus) do not drop to zero.

2.3. Smooth and nonsmooth tipping In general, parameters are not static in climate models of this type, but rather can oscillate seasonally and have a mean that can drift over time due to climatic variation. As an example, the fresh water hosing from the melting of the Arctic ice leads to variation in η_2 of exactly this nature. To capture the impact of such parameter variation, we consider the case where $\eta_2(t)$ is time dependent, with a mean drift of rate ϵ, and a seasonal oscillation of amplitude A and frequency ω, so that

$$\eta_2(t) = \eta_{2,0} - \epsilon t + A\sin(\omega t). \tag{2.3}$$

Thus,

$$\dot{\mathcal{V}} = \eta_1 - \eta_2(t) + \eta_3(\mathcal{T} - \mathcal{V}) - \mathcal{T} - \mathcal{V}|\mathcal{V}|, \quad \dot{\mathcal{T}} = \eta_1 - \mathcal{T}(1 + |\mathcal{V}|), \tag{2.4}$$

https://doi.org/10.1017/S1446181125100114 Published online by Cambridge University Press

with $\eta_2(t)$ given by (2.3). As is typical for applied settings [8], we follow certain parameter assumptions. It is frequently assumed that the salinity's relaxation time is much longer than that of temperature, giving $\eta_3 < 1$, which results in an SNB in (2.4) for the branch $\mathcal{V} > 0$. Furthermore, we take $\eta_1 = O(1)$ so that $\eta_{2c} = \eta_3\eta_1 = O(1)$ and $\eta_{2c} < \eta_{2sf}$. That is, there is a nontrivial bi-stability range for the two stable equilibria on the branches **N** ($\mathcal{V} > 0$) and **F** ($\mathcal{V} < 0$), as shown in Figure 1. Variation of a parameter (typically η_2 in (2.2) as given by (2.3)) can lead to tipping, which in the context of this study corresponds to a solution starting at the focus **F** (or **N**) that does not stay close to **F** (or **N**) but rapidly evolves to a qualitatively different state, typically to **N** (or **F**) or to a large amplitude periodic orbit.

2.3.1. Smooth B-tipping If η_2 is slowly *increased* through the SNB η_{2sn} at a constant rate $d\eta_2/dt = \epsilon \ll 1$, then we see *canonical B-tipping* with a transition from a stable temperature-dominated state (N) to a stable salinity-dominated state (F). Such tipping is described by standard theory [10] and occurs at the point

$$\eta_2 = \eta_{2sn} + C_{sn}\,\epsilon^{2/3}. \tag{2.5}$$

In this expression, $C_{sn} > 0$, so that the tipping point is delayed till after the bifurcation (with obvious climatic implications).

2.3.2. Nonsmooth B-tipping In contrast, if η_2 is slowly *decreased* through the nonsmooth fold at η_{2sf} at a constant rate $d\eta_2/dt = -\epsilon$, then nonsmooth B-tipping occurs, with a transition from F to N. This is illustrated in Figure 1, where we can see the lag in the tipping. B-tipping close to an NSF is different in many respects from B-tipping close to an SNB, partly because the eigenvalues of the linearization of the nonsmooth system about the fixed point do not drop to zero at a border collision bifurcation. We show presently (see also the related 1D model discussed in [6]) that B-tipping occurs for the nonsmooth system, in the sense that $|V| = K \gg 1$, at the parameter value

$$\eta_2 = \eta_{2sf} - C_{sf}\,\epsilon \log(K/\epsilon), \quad C_{sf} > 0.$$

Observe that the expression for the lag in the tipping point scales differently from the smooth case in (2.5).

The case of B-tipping due to seasonal forcing (possibly combined with slow drift) is more subtle and, as in the 1D case, is dominated by the existence of a cyclic-fold bifurcation which can lead to an advancement of the tipping point. In [6], this was explored for an NSF in a 1D simplification of (2.2) and a pattern of tipping not dissimilar to the smooth case was observed. However, in the case of the full 2D problem (2.2), there are additional effects due to the possibility of resonance between the seasonal parameter variation and the natural frequency of the focus. This can lead to complex behaviour close to the tipping point, including chaotic dynamics. This behaviour is unique to the NSF and cannot occur at a standard SNB as there is no natural frequency in the latter case.

https://doi.org/10.1017/S1446181125100114 Published online by Cambridge University Press

3. The normal form of the Stommel 2-box model close to an NSF as a forced piece-wise smooth system

3.1. Overview Our primary interest in this paper is the nature of the tipping of the system (2.4) close to the nonsmooth saddle-focus (border collision) bifurcation. Accordingly, we track the system (2.4) near the two respective fixed points. Following an expansion around each fixed point, we find that, to leading order, the Stommel 2-box model can be simplified to a piece-wise linear normal form. This is a continuous dynamical system comprising two linear systems, separated by the surface $\Sigma \equiv \{\mathcal{V} = 0\}$ across which the solution trajectory loses smoothness. We find that the properties of the linear operators of each of the two linearized equations play a critical role in the resulting dynamics. Here, we provide a summary of the linearized system and its elementary properties.

Consider the Stommel 2-box model (2.4). At the nonsmooth fold, we have $\mathcal{V} = 0$ and $\mathcal{T} = \eta_1$. We set $\mathcal{V} = V \ll 1$ and $\mathcal{T} = \eta_1 + T$ with $T \ll 1$, and take

$$\eta_2(t) = \eta_1\eta_3 + \theta(t) \equiv \eta_{2sf} + \theta(t),$$

where from (2.3), we express the parameter drift and seasonal forcing by

$$\theta(t) \equiv \mu(t) + A\sin(\omega t) \equiv \mu_0 - \epsilon t + A\sin(\omega t),$$

so that a static border collision bifurcation occurs when $\mu = \epsilon = A = 0$. Furthermore, let

$$\mathbf{x} = (T, V)^T, \quad \mathbf{e}_1 = (1, 0)^T, \quad \mathbf{e}_2 = (0, 1)^T. \tag{3.1}$$

The Stommel 2-box model is smooth in the respective regions

$$S^+ = \{x \mid \mathbf{e}_2^T\mathbf{x} = V > 0\}, \quad S^- = \{\mathbf{x} \mid \mathbf{e}_2^T\mathbf{x} < 0\},$$

and loses smoothness across the discontinuity set

$$\Sigma = \{x \mid \mathbf{e}_2^T\mathbf{x}\} = 0.$$

Close to the NSF, the Stommel 2-box model then simplifies to the piece-wise linear normal form

$$\dot{\mathbf{x}} = L^{\pm}\mathbf{x} - \theta(t)\,\mathbf{e}_2, \tag{3.2}$$

where the linear operators

$$L^+ = \begin{pmatrix} -1 & -\eta_1 \\ \eta_3 - 1 & -\eta_3 \end{pmatrix}, \quad L^- = \begin{pmatrix} -1 & \eta_1 \\ \eta_3 - 1 & -\eta_3 \end{pmatrix},$$

are respectively applied in the regions S^+ and S^-.

Hence, the (forced) Stommel 2-box model (2.4) has the normal form

$$\dot{\mathbf{x}} = L^{\pm}\mathbf{x} - (\mu(t) + A\sin(\omega t))\,\mathbf{e}_2 \equiv L^{\pm}\mathbf{x} - (\mu_0 - \epsilon t + A\sin(\omega t))\,\mathbf{e}_2. \tag{3.3}$$

https://doi.org/10.1017/S1446181125100114 Published online by Cambridge University Press

We study the normal form (3.3) in detail for the remainder of this paper, looking at the cases of:

(i) drift-induced tipping close to $\mu = 0$ when $A = 0$;
(ii) seasonal tipping when $\epsilon = 0$ with ω large, small and resonant; and
(iii) combined tipping when ϵ and A are both nonzero.

We first derive some elementary properties of this piece-wise linear system (3.2) which we will refer to in the later Sections 4, 5 and 6.

3.2. Fixed points It is immediate that if $\mu(t) = \mu \equiv \mu_0$ is fixed, then there are fixed points, a saddle $\mathbf{S} = \mu\,\mathbf{s}$ and a focus $\mathbf{F} = \mu\,\mathbf{f}$ given by

$$\mathbf{s} = (L^+)^{-1}\mathbf{e}_2 = \frac{1}{\eta_3 + \eta_1(\eta_3 - 1)}\begin{pmatrix}\eta_1\\ -1\end{pmatrix}, \quad \mathbf{f} = (L^-)^{-1}\mathbf{e}_2 = \frac{1}{\eta_3 - \eta_1(\eta_3 - 1)}\begin{pmatrix}-\eta_1\\ -1\end{pmatrix}. \tag{3.4}$$

Observe, as expected, that if $0 < \eta_3 < 1$ and $\eta_1 \gg \eta_3$, then $S \in S^+$ and $F \in S^-$ if and only if $\mu > 0$, with the BCB occurring at $\mu = 0$. The resulting phase plane of the linearized system (3.3) either side of the NSF in the case where $A = 0$ and $\mu = \pm 1$ is given in Figure 2. In this figure, the (physical) saddle is indicated by an o and the focus (when $\mu > 1$) is clear from the limits of the trajectories.

We observe, trivially, that in contrast to the SNB, the linearization of the system (3.2) about the fixed points is *independent of the value of* μ. The corresponding linear operators $L^\pm$ have eigenvalues $\sigma^\pm_{1,2}$ and eigenvectors $\mathbf{u}^\pm_{1,2}$, where

$$\sigma^\pm_1 + \sigma^\pm_2 = -(1 + \eta_3), \quad \sigma^\pm_1\sigma^\pm_2 = \eta_3 \pm \eta_1(\eta_3 - 1),$$

so that if $\eta_3 \ll 1$,

$$\sigma^\pm_1 = -\tfrac{1}{2} + \tfrac{1}{2}\sqrt{1 \pm 4\eta_1}, \quad \sigma^\pm_2 = -\tfrac{1}{2} - \tfrac{1}{2}\sqrt{1 \pm 4\eta_1}.$$

Hence, for the typical range of η_1, η_3, we have that $\sigma^+_{1,2}$ are real with $\sigma^+_1 > 0 > \sigma^+_2$, and $\sigma^-_{1,2}$ are complex with negative real part. For most of this paper, we will consider the representative values of

$$\eta_1 = 3, \quad \eta_3 = 0.3.$$

In this case,

$$\sigma^+_1 = 0.84\cdots, \quad \sigma^+_2 = -2.14\cdots, \quad \sigma^-_1 = -0.65\cdots + 1.41\cdots\, i,$$
$$\sigma^-_2 = -0.65\cdots - 1.41\cdots\, i.$$

Accordingly, we may expect resonant behaviour in the system when the forcing frequency is close to the frequency of the focus and satisfies $\omega \approx 1.4$.

3.3. Smooth periodic orbits in S^- and grazing Now, consider the case of μ fixed and seasonal forcing with $A > 0$. Provided A/μ is sufficiently small, the system (3.3) has a *smooth and stable periodic solution* lying wholly in S^-. A straightforward

https://doi.org/10.1017/S1446181125100114 Published online by Cambridge University Press

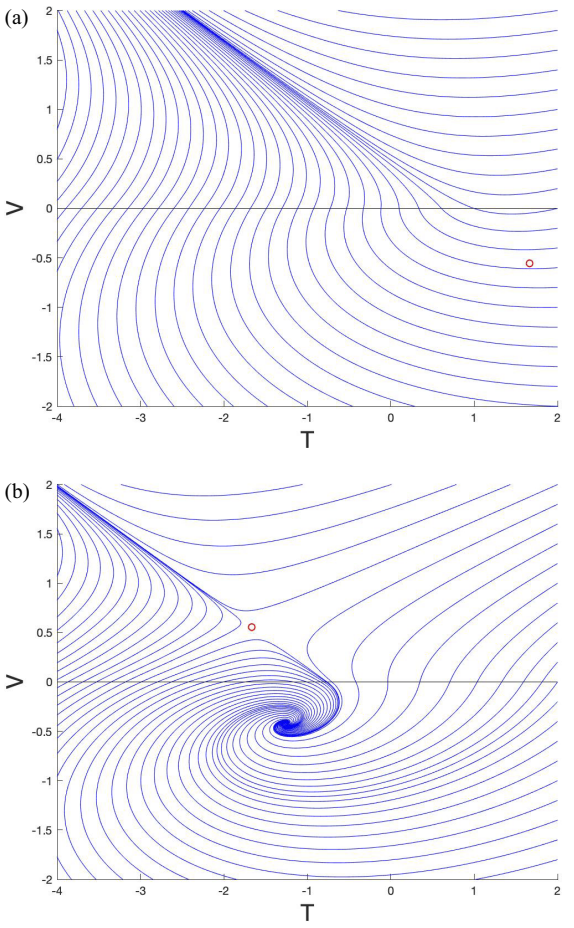

FIGURE 2. Solutions of the linearized problem (3.3) in the (T, V) phase plane when $A = 0$. (a) $\mu = -1$. The (unphysical) saddle is shown as an o. (b) $\mu = 1$ showing the (physical) saddle as an o and the stable focus.

calculation shows that the periodic orbit is given by

$$\mathbf{P}^-(t) = \mu\mathbf{f} + A(\omega^2 I + (L^-)^2)^{-1}\left[\omega\cos(\omega t)\mathbf{e}_2 + \sin(\omega t)L^-\mathbf{e}_2\right].$$

It also has a smooth unstable periodic orbit lying wholly in S^+ given by

$$\mathbf{P}^+(t) = \mu\mathbf{s} + A(\omega^2 I + (L^+)^2)^{-1}\left[\omega\cos(\omega t)\mathbf{e}_2 + \sin(\omega t)L^+\mathbf{e}_2\right]. \tag{3.5}$$

Both orbits play a critical role in understanding tipping close to the NSF under seasonal forcing.

https://doi.org/10.1017/S1446181125100114 Published online by Cambridge University Press

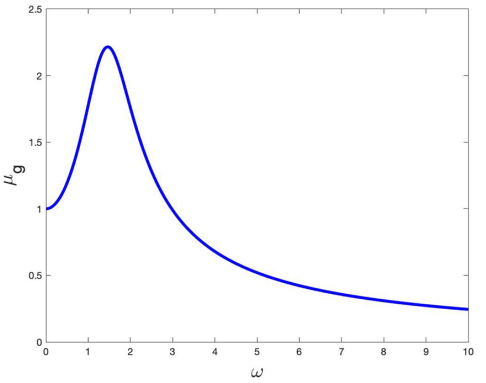

FIGURE 3. The grazing value μ_g, when $A = 1, \eta_1 = 3, \eta_3 = 0.3$.

If $\omega \gg 1$, then we have to leading order that the stable periodic orbit is given by

$$\mathbf{P}^-(t) = \mu\mathbf{f} + A\frac{\cos(\omega t)}{\omega}\mathbf{e}_2.$$

This periodic orbit lies wholly in S^- provided that

$$\frac{A}{\mu} < \omega|\mathbf{e}_2^T\mathbf{f}|. \tag{3.6}$$

Similarly, if $\omega \ll 1$, then to leading order, the periodic orbit is given by

$$\mathbf{P}^-(t) = \mu\mathbf{f} + A\sin(\omega t)\mathbf{f}. \tag{3.7}$$

This orbit lies wholly in S^- provided that

$$\frac{A}{\mu} < 1,$$

and if $A/\mu = 1$, it touches the origin.

The stable periodic orbit $\mathbf{P}^-(t)$ in S^- will have its largest amplitude when ω is close to the resonant value of $\omega = \beta$. (Note that resonance is not important in S^+.)

In general, as μ is decreased from a large value (or equivalently, as A is increased from zero), then there will be a first value μ_g (equivalently A_g) when the periodic solution $\mathbf{P}^-(t)$ *grazes* the line Σ. This occurs when $\max(\mathbf{e}_2{}^T\mathbf{P}^-(t)) = 0$. As μ is decreased through μ_g (A is increased), the periodic orbit will persist before vanishing at a cyclic fold at $\mu = \mu_c$. At this point, we see cyclic B-tipping or more complex behaviour. We consider this case presently. We present in Figure 3 a plot of the (grazing) value μ_g as a function of ω in the case of $A = 1, \eta_1 = 3, \eta_3 = 0.3$. Note that μ_g takes its largest value at the resonant frequency $\omega \approx 1.4$. We deduce that μ_g increases close to the resonant value and, for these values of ω, we expect to see significantly advanced tipping. This is quite different from tipping in the 1D map case studied in [6].

https://doi.org/10.1017/S1446181125100114 Published online by Cambridge University Press

4. Drift-induced B-tipping

We first consider the case of drift-only-induced tipping when $A = 0$ for which $\mu(t) = \mu_0 - \epsilon t$ and we take $\mathbf{x}(0) = \mu_0 \mathbf{f}$. The analysis is similar to the 1D case [6] and is also given in [5].

To make the calculations of tipping precise, we observe that as the normal form we are considering is a piece-wise linear system, any divergence to infinity of the solution occurs only in infinite time (unlike the case of tipping close to an SNB where (owing to the quadratic form of the nonlinearity) the divergence to infinity takes place in finite time). In the case of the piece-wise linear normal form, we (as described earlier) define tipping, in this and future sections, to have occurred when

$$\mathbf{e}_2^T \mathbf{x} = V = K$$

for some suitably large $K > 0$ (typically, we take $K = 10$). A similar definition of tipping for a 1D piece-wise linear system was used in [6].

The estimate (4.1) agrees well with numerical experiments for small values of ϵ. In Figure 4, we present the tipping value of μ calculated numerically (blue) and the estimate (4.1) (red) for the case of $\eta_1 = 3, \eta_3 = 0.3$, for which $1/\sigma_1 = 1.18$.

The form of the tipping: (i) as a function of $\mu(t)$ and (ii) in the (T, V) phase plane, is shown in Figure 5. When $\mathbf{x} \in S^-$, and ignoring rapidly decaying exponential terms, the trajectory takes the form

$$\mathbf{x}^-(t) = \mu(t)\mathbf{f} - \epsilon (L^-)^{-1}\mathbf{f}.$$

This trajectory intersects the discontinuity set Σ at the time t_1 when $\mu(t_1) = \epsilon\, \mathbf{e}_2^T[(L^-)^{-1}\mathbf{f}]/\mathbf{e}_2^T\mathbf{f}$. It then enters S^+, where (again ignoring rapidly decaying terms) it takes the form

$$\mathbf{x}^+(t) = \mu(t)\mathbf{s} - \epsilon (L^+)^{-1}\mathbf{s} + a\, \epsilon\, e^{\sigma_1^+(t-t_1)}\, \mathbf{u}_1^+,$$

where the eigenvalue σ_1^+ is as given in Section 3, and the precise value of a is given by matching $\mathbf{x}^-$ to $\mathbf{x}^+$ on Σ. The dominant feature of this expression is the exponentially growing term parallel to the eigenvector $\mathbf{u}_1^+$ of L^+ (as can be seen in Figure 5). Accordingly, we predict that B-tipping occurs, to leading order in ϵ, when

$$\mu = -\frac{\epsilon}{\sigma_1}\, \log(K/\epsilon) + O(\epsilon). \tag{4.1}$$

5. High-frequency B-tipping when μ is fixed and $\omega \gg 1$

In this section, we consider high-frequency periodic forcing with no drift, so that μ is fixed, with $\epsilon = 0$ and $\omega \gg 1$. This case was first considered in [5] and also in [6], and we extend the results obtained in these papers. The main result is then given in the following proposition.

https://doi.org/10.1017/S1446181125100114 Published online by Cambridge University Press

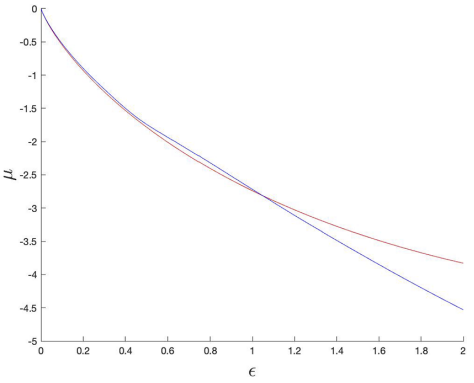

FIGURE 4. Drift-induced tipping comparing the calculated tipping point μ (blue) with the estimate (4.1) (red).

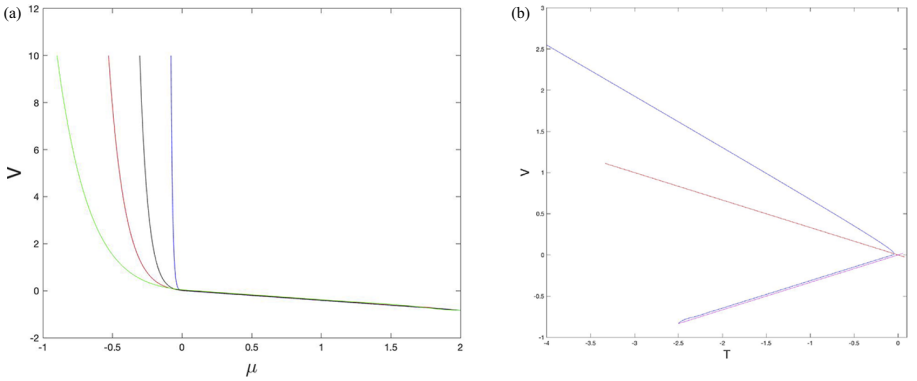

FIGURE 5. (a) Drift-induced B-tipping as a function of μ for a range of values of $\epsilon = 0.2, 0.1, 0.05, 0.01$ and with $K = 10$ (from left to right respectively in green, red, black and blue). (b) Tipping (blue trajectory) in the (T, V) phase plane when $\epsilon = 0.05$. In this figure, the locus of the two points $\mu\mathbf{f} \in S^-$ and $\mu\mathbf{s} \in S^+$ are shown in red.

PROPOSITION 5.1. *Let the parameter λ be defined by*

$$\lambda = \frac{A}{\omega\mu}.$$

Then, we have the following results.

(i) *For $\lambda < \lambda_g = |\mathbf{e}_2^T\mathbf{f}|$, the system (3.2) has a stable periodic solution lying entirely within S^- centred on the focus $\mu\mathbf{f}$. As λ is decreased to $\lambda = \lambda_g$, this orbit grazes Σ.*

(ii) *For $\lambda_g < \lambda < \lambda_c$, the stable periodic orbit persists and lies in both S^- and S^+, and for $\lambda_g < \lambda = \lambda_0 < \lambda_c$, it has a figure-of-eight form centred on $V = 0$.*

(iii) *At $\lambda = \lambda_c$, the stable periodic orbit ceases to exist at a cyclic fold bifurcation. For $\lambda > \lambda_c$, the solution diverges to infinity and we see tipping behaviour.*

https://doi.org/10.1017/S1446181125100114 Published online by Cambridge University Press

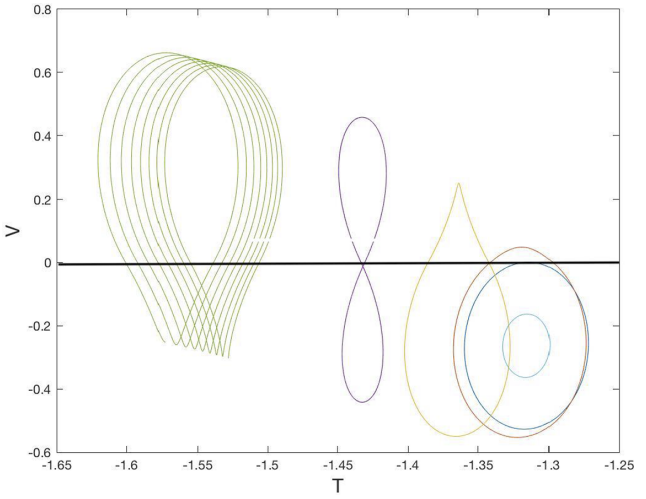

FIGURE 6. The behaviour under high-frequency periodic forcing with $\omega = 10$ and $\eta_1 = 3, \eta_3 = 0.3$. Parameter values: $\lambda_g = 0.416, \lambda_0 = 0.748$ and $\lambda_c = 0.767$. This shows the stable periodic orbits that exist for $\lambda = 0.4, 0.5, 0.6, 0.75, 0.76$ (respectively cyan, blue, red, orange, mauve). Observe that the centre of the periodic orbit shifts to the left when it lies on both sides of Σ and in the case of the symmetric figure-of-eight orbit, it is centred on $V = 0, T = -1/(1 - \eta_3)$. For larger $\lambda = 0.77 > \lambda_c$, the stable periodic orbit ceases to exist and, instead, the solution diverges to infinity (tipping behaviour). This behaviour is seen in the left-most orbit in the figure. The discontinuity set $V = 0$ is indicated.

The conclusions of Proposition 5.1 are illustrated in Figure 6. In this figure, we take $\omega = 10$ and plot the stable periodic orbit for different values of $\lambda < \lambda_c$ and an orbit (left-most) for λ just greater than λ_c, which is diverging to infinity. We see the transition from a near-circular orbit wholly in S^- to a figure-of-eight orbit for λ slightly smaller than λ_c, and then to a solution which diverges to infinity (tipping behaviour) as λ increases.

We now derive the results in this proposition. Result (i) follows immediately from the results described in Section 3.2.

To derive the other results for large ω, we set $\mathbf{x} = \mu\mathbf{z}$, $\lambda = A/(\omega\mu)$ and $\tau = \omega t$. Under rescaling, the linear normal form of the Stommel 2-box model becomes

$$\dot{\mathbf{z}} = L^{\pm}\,\mathbf{z}/\omega - \lambda \sin(\tau)\mathbf{e}_2 - \mathbf{e}_2/\omega.$$

We assume that $\lambda = O(1)$ and set

$$\mathbf{z} = \mathbf{z}_0 + \mathbf{z}_1/\omega + \cdots .$$

We then have, for some constant vector $\mathbf{C} = [C_1, C_2]^T$ (to be estimated at the next level of the asymptotics),

$$\mathbf{z}_0(\tau) = \mathbf{C} + \lambda \cos(\tau)\mathbf{e}_2. \tag{5.1}$$

https://doi.org/10.1017/S1446181125100114 Published online by Cambridge University Press

Hence, $\mathbf{z}_0(\tau)$ is a periodic orbit centred on $\mathbf{C}$. Observe that in this limit, $\mathbf{z}_0(\tau)$ only oscillates in the V direction parallel to $\mathbf{e}_2$. If $\lambda < |C_2|$, this periodic orbit lies wholly in S^-.

At the next level of asymptotics,

$$\dot{\mathbf{z}}_1 = L^{\pm}\mathbf{z}_0 - \mathbf{e}_2. \tag{5.2}$$

This differential equation admits a periodic solution provided that

$$\mathbf{I} \equiv \int_0^{2\pi} L^{\pm}\mathbf{z}_0 \, d\tau = 2\pi\mathbf{e}_2. \tag{5.3}$$

We use this identity to determine $\mathbf{C}$. It is immediate that ${\mathbf{e}_2}^T\mathbf{z}_0 = C_2 + \lambda\cos(\tau)$. Hence, the choice of $\pm$ in the integrand (5.3) depends only upon C_2. The following results are immediate:

$$ {\mathbf{e}_2}^T L^{\pm}\mathbf{e}_2 = -\eta_3, \quad {\mathbf{e}_1}^T L^{\pm}\mathbf{e}_2 = \mp\eta_1, \quad L^{\pm}\mathbf{e}_1 = (-1, \eta_3 - 1), \tag{5.4}$$

where $\mathbf{e}_1$ and $\mathbf{e}_2$ are as defined in (3.1). Multiplying $\mathbf{I}$ by ${\mathbf{e}_2}^T$ and applying (5.4) gives

$$(\eta_3 - 1)C_1 - \eta_3 C_2 = 1.$$

We now make some estimates for C_1 and C_2 which allow us to deduce the existence of the cyclic fold at $\lambda = \lambda_c$.

LEMMA 5.2.

(i) *In general,*

$$2\pi\, C_1 = -\eta_1 \int_0^{2\pi} |C_2 + \lambda\cos(\tau)| \, d\tau < 0.$$

(ii) *If $\lambda < |C_2|$, then the periodic orbit $\mathbf{z}_0$ lies only in S^- and $C_1 = -\eta_1|C_2|$.*

(iii) *If $\lambda > |C_2|$, then the periodic orbit $\mathbf{z}_0$ lies in both S^- and S^+, and we have*

$$C_1 = -\frac{2\eta_1}{\pi}\Big[\sqrt{\lambda^2 - C_2^2} + C_2 \sin^{-1}(C_2/\lambda)\Big].$$

PROOF. (i) To obtain this identity, we multiply $\mathbf{I}$ by ${\mathbf{e}_1}^T$. This gives

$$-2\pi C_1 + \int_0^{2\pi} \mp\eta_1(C_2 + \lambda\cos(\tau)) \, d\tau = 0.$$

However, by definition, the sign of $C_2 + \lambda\cos(\tau)$ is precisely the opposite of the sign of $\mp$. Hence, the result (i). Results (ii) and (iii) follow by direct quadrature. □

We now consider the effect of increasing λ from zero to a maximum value at which there is a cyclic-fold bifurcation.

If $\lambda < |C_2|$, the periodic orbit lies only in S^-, and from the earlier results (3.4), (3.6),

$$C_1 = -\eta_1/(\eta_3 - \eta_1(\eta_3 - 1)), \quad C_2 = -1/(\eta_3 - \eta_1(\eta_3 - 1)) < 0,$$
$$\lambda_g = 1/(\eta_3 - \eta_1(\eta_3 - 1)).$$

https://doi.org/10.1017/S1446181125100114 Published online by Cambridge University Press

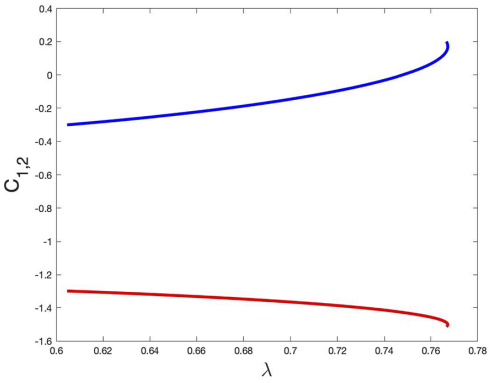

FIGURE 7. The values of C_1 (red) and C_2 (blue) as a function of λ when $\eta_1 = 3$ and $\eta_3 = 0.3$. The cyclic fold is clearly visible and occurs when $(\lambda_c, C_2) = (0.7672, 0.17)$.

Now, consider the case of $\lambda > \lambda_g$ when the periodic orbit lies both in S^+ and S^-. Combining the results above, we have that C_2 satisfies the identity

$$-\frac{2\eta_1(\eta_3-1)}{\pi}\Big[\sqrt{\lambda^2-C_2^2}+C_2\sin^{-1}(C_2/\lambda)\Big]-\eta_3 C_2 = 1. \tag{5.5}$$

The solution C_2 of this together with C_1 is plotted in Figure 7. We see that this has a (cyclic-)fold bifurcation with λ taking its largest value λ_c when $dC_2/d\lambda = 0$ for a small value of $C_2 > 0$. For the case plotted of $A = 1, \eta_1 = 3, \eta_3 = 0.3$, we have $(\lambda_c, C_2) = (0.7672, 0.17)$.

LEMMA 5.3.

(i) $C_2 = 0$ *if*

$$\lambda \equiv \lambda_0 = \frac{\pi}{2\eta_1(1-\eta_3)}, \quad C_1 = \frac{1}{\eta_3 - 1}.$$

(ii) *If* $\eta_3 \ll 1$, *then* λ *takes its maximum values* $\lambda = \lambda_c$, *when*

$$\frac{1}{\lambda_c} = \frac{2\eta_1(1-\eta_3)}{\pi} - \frac{\pi\eta_3^2}{4\eta_1(1-\eta_3)}, \quad C_2 = \frac{\eta_3\pi\lambda_c}{2\eta_1(1-\eta_3)} \ll 1. \tag{5.6}$$

PROOF. Result (i) follows by inspection. To establish result (ii), we first assume that C_2 is small. We then approximate (5.5) by the quadratic equation

$$-\frac{2\eta_1(\eta_3-1)}{\pi}\Big(\lambda+\frac{C_2^2}{2\lambda}\Big)-\eta_3 C_2 = 1.$$

Hence, in this limit,

$$\frac{1+\eta_3 C_2}{(1-\eta_3)} = \frac{2\eta_1}{\pi}\Big(\lambda+\frac{C_2^2}{2\lambda}\Big).$$

https://doi.org/10.1017/S1446181125100114 Published online by Cambridge University Press

This quadratic equation has a fold bifurcation at $\lambda = \lambda_c$ when its discriminant vanishes. This gives the expressions for λ_c and C_2 in (5.6). Note that if $\eta_3 \ll 1$, then $C_2 \ll 1$, justifying the assumptions made. □

We conclude that the periodic solution z_0 vanishes in a *cyclic-fold bifurcation* for $\lambda = \lambda_c$. For $\lambda > \lambda_c$ in this high-frequency limit, we do not have a stable periodic solution and (cyclic) B-tipping occurs. Equivalently, this tipping occurs if $A > A_c$ or if $\mu < \mu_c$.

To complete the calculation of the form of the periodic solution, we explain the figure-of-eight shape of the orbit which occurs when $\lambda = \lambda_0$ and is shown in Figure 6. The first-order contribution to the periodic orbit is given by $\mathbf{z}_1(\tau)$ which satisfies the ordinary differential equation (ODE) (5.2) using (5.1),

$$\dot{\mathbf{z}}_1 = L^{\pm}(C_1\mathbf{e}_1 + (C_2 + \lambda\cos(\tau)\mathbf{e}_2)) - \mathbf{e}_2.$$

Let $\mathbf{z}_1 = (p, q)^T$. By taking projections, we find that

$$\dot{p} = -C_1 - \eta_1|C_2 + \lambda\cos(\tau)|, \quad \dot{q} = (\eta_3 - 1)C_1 - \eta_3 C_2 - 1 - \eta_3\lambda\cos(\tau).$$

As $(\eta_3 - 1)C_1 - \eta_3 C_2 - 1 = 0$, we see that q simply oscillates in phase with $\mathbf{z}_0$. Now, consider p. If $|C_2|$ is sufficiently large, then $C_2 - \lambda\cos(\tau)$ takes one sign only. Hence, p has the same frequency of oscillation as $\mathbf{z}_0$. The orbits in this case will be elliptical, as we can see in the numerical calculation presented in Figure 6. In contrast, if $|C_2|$ is small and, in particular, if $\lambda = \lambda_0, C_2 = 0$, the function $|\lambda\cos(\tau)|$ is a "rectified cosine wave". This has period π, half that of the function $\cos(\tau)$. Indeed, to a first Fourier mode approximation,

$$|\cos(\tau)| \approx \cos^2(\tau) = \tfrac{1}{2}(1 + \cos(2\tau)).$$

Thus, in this case, p has half the period of $\mathbf{z}_0$, which gives the figure-of-eight curve observed in this case in Figure 6.

6. Low-frequency periodic forcing with no drift

Suppose now that $\omega \ll 1$. We have shown in Section 3.2 (3.7) that in the case of small ω and for sufficiently large μ, the orbit in S^- takes the leading-order form

$$P^-(t) = \mathbf{x}(t) = [\mu + A\sin(\omega t)]\,\mathbf{f}.$$

As μ decreases, at $\mu = \mu_g \approx A$, this orbit touches Σ close to the origin. For smaller values of μ, this trajectory enters the region S^+, where it becomes subject to the exponential growth arising from the positive eigenvalue of the linear operator L^+. Then, for such a periodic orbit to exist in this range, it must spend a short time in

https://doi.org/10.1017/S1446181125100114 Published online by Cambridge University Press

S^+, limiting the effect of the exponential growth, before returning to the region S^-. At a value $\mu_c < \mu_g$, the periodic orbit loses stability at a cyclic-fold.

To pursue the construction of the periodic orbit, we consider first a scaling argument. Setting $\tau = \omega t$ with $\omega \ll 1$ gives

$$\omega\, \mathbf{x}_\tau = L^{\pm}\mathbf{x} - (\mu + A\sin(\tau))\mathbf{e}_2.$$

To leading order in (small) ω, noting from Section 3.1 that $\mathbf{s} = (L^+)^{-1}\mathbf{e}_2$ and $\mathbf{f} = (L^-)^{-1}\mathbf{e}_2$, we then have

$$\mathbf{x} = \mu(1 + \sin(\tau))\mathbf{f} \quad \text{or} \quad \mathbf{x} = \mu(1 + \sin(\tau))\mathbf{s}.$$

Hence, the orbit will be "L-shaped" with two sections meeting close to the origin, a longer one in S^- parallel to $\mathbf{f}$ and a shorter one in S^+ parallel to $\mathbf{s}$. Examples of such periodic orbits, when $A = 1, \eta_1 = 3, \eta_3 = 0.3$ with $\omega = 0.1, \mu = 1.008$ and $\omega = 0.25, \mu = 1.007$, are shown in Figure 8, where the dynamics in the respective regions S^- and S^+ is close to being parallel to the vectors $\mathbf{f}$ and $\mathbf{s}$.

In the region S^+, we see linear dynamics associated with the linear operator L^+. This operator has eigenvalues $\sigma_1^+ > 0 > \sigma_2^+$ with corresponding eigenvectors $\mathbf{u}_1^+$ and $\mathbf{u}_2^+$. The corresponding dynamics in S^+ is then given by

$$\mathbf{x}(t) = \mu\mathbf{s} + \alpha_1 e^{\sigma_1^+ t}\mathbf{u}_1^+ + \alpha_2 e^{\sigma_2^+ t}\mathbf{u}_2^+ + A(\omega^2 I + (L^+)^2)^{-1}(\omega\cos(\omega t)\mathbf{e}_2 + \sin(\omega t)L^+\mathbf{e}_2),$$

so that expanding in ω, we have the following expression for the trajectory:

$$\mathbf{x}(t) = \mu(1 + (A/\mu)\sin(\tau))\mathbf{s} + \omega\cos(\tau)(L^+)^{-1}\mathbf{s} + \alpha_1 e^{\sigma_1^+\tau/\omega}\mathbf{u}_1^+ + \alpha_2 e^{\sigma_2^+\tau/\omega}\mathbf{u}_2^+ + O(\omega^2). \tag{6.1}$$

A similar expression for the trajectory applies in the region S^-.

The trajectory (6.1) enters S^+ close to the origin and moves towards $\mathbf{s}$, but returns to Σ due to the effect of the term $\alpha_1 \exp(\sigma_1^+\tau/\omega)\mathbf{u}_1^+$. Because of this strong exponential growth in the region S^+, the orbit can only remain in this region for a scaled time of $\tau = O(\omega)$. As a consequence, the deviation of the orbit in the direction towards $\mathbf{s}$ is also $O(\omega)$. It follows that if $\mathbf{x}$ leaves and returns to the set Σ in this time, then α_1 and α_2 must also both be of $O(\omega)$. Hence, the length and the width of the orbit in S^+ are $O(\omega)$. Similarly, the orbit is of approximate length 2μ in S^-. This behaviour can be clearly seen in Figure 8 when we compare the solutions for $\omega = 0.1$ and $\omega = 0.25$.

In Figure 9, we present numerical experiments for small $\omega < 0.5$ in which we calculate the value of μ_c at which the periodic orbit loses stability, and compare this value with the grazing point μ_g and a fitted parabola. In this and later calculations of μ_c, we calculate the stable periodic orbit at μ_g numerically (using the Matlab routine ode15s) as the ω-limit set of the trajectory starting from the focus $\mathbf{F}$. We then systematically reduce μ, following the orbit, until it loses stability at μ_c.

From examining this figure, we conclude that if $\omega < 0.35$, there is a reasonable fit to a parabola so that

$$\mu_c \approx A(1 + C\,\omega^2), \quad C > 0,$$

https://doi.org/10.1017/S1446181125100114 Published online by Cambridge University Press

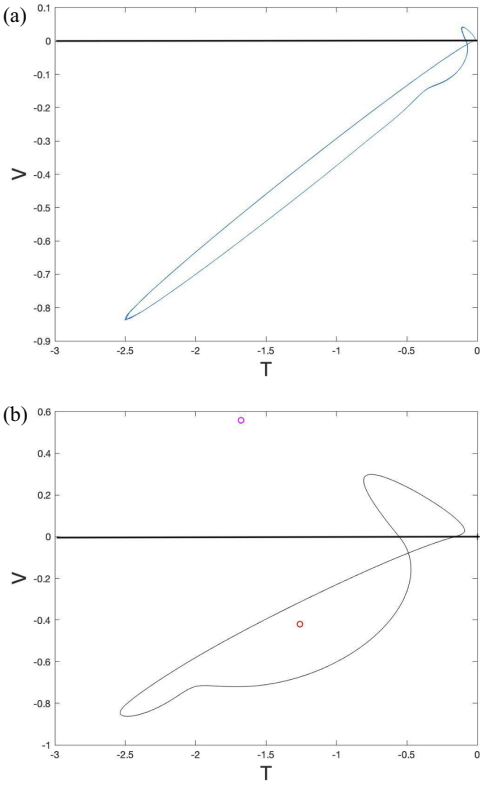

FIGURE 8. Periodic orbits for small ω: (a) $\omega = 0.1, \mu = 1.0008$; (b) $\omega = 0.25, \mu = 1.007$. The two fixed points $\mu\mathbf{f}$ and $\mu\mathbf{s}$ are shown circled. Observe the broadening of the orbit as ω increases. The discontinuity set $V = 0$ is indicated.

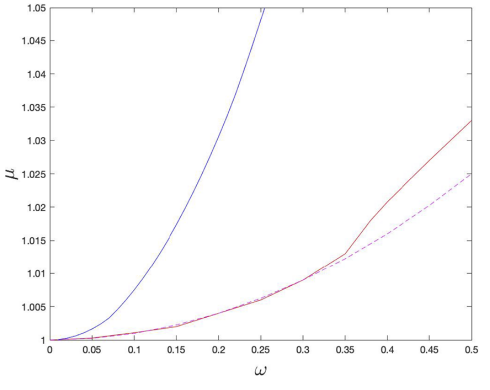

FIGURE 9. The small ω values of the grazing point μ_g (blue), the tipping point μ_c (red) and the fitted parabolic estimate $(1 + 0.1\omega^2)$ (dashed magenta) when $A = 1, \eta_1 = 3, \eta_3 = 0.3$.

https://doi.org/10.1017/S1446181125100114 Published online by Cambridge University Press

where for $\eta_1 = 3, \eta_3 = 0.3$, we have $C \approx 0.1$. For $\omega > 0.35$, the values of μ_c depart from the fitted parabolic curve, as the effect of resonance at $\omega \approx 1$ becomes more important.

7. Near-resonant periodic forcing with no drift

Having studied the periodic orbit for the large and small ω limits, we now look at forcing frequencies in the range of $\omega = O(1)$. Of special interest are values close to the natural frequency of the focus in S^-, which for the canonical values of the parameters is given by $\omega = 1.4$. The resonance linked to this leads to significantly more complex behaviour than the cases of small- and large-ω studies earlier, with a more complicated path to tipping as μ is decreased from μ_g. We see the "simple" orbit at $\mu = \mu_g$ develop additional structure through (possibly a sequence of) bifurcations, leading to (possibly) chaotic behaviour. The chaotic attractor then loses stability as μ decreases, giving rise to tipping.

To illustrate this, we fix $\omega = 1$ and consider a range of orbits as we decrease μ towards a tipping value estimated to be $\mu \equiv \mu_c = 1.205$. These orbits are shown in Figure 10. We see here very different behaviour from before. In particular, as μ decreases, the "simple" periodic orbit does not vanish at a cyclic fold bifurcation. Instead, it has a period-doubling bifurcation at $\mu \approx 1.27$ evolving, through more bifurcations and the creation of extra loops, into a (stable) chaotic orbit as μ decreases. This chaotic orbit then ceases to exist at μ_c leading to tipping. The corresponding bifurcation diagram is shown in Figure 11(a) for $\omega = 1$. This diagram is obtained for each μ by evolving the orbit forward till it reaches its ω-limit set and then plotting V at time intervals $t_n = 2n\pi/\omega$. In Figure 11(b), we contrast this with a similar bifurcation diagram when $\omega = 1.2$. In this, we also see a single period-doubling bifurcation, but the period-two orbit then becomes unstable to tipping at $\mu_c = 1.17$ without evolving into a chaotic attractor.

Because of the complexity of the behaviour close to resonance, the calculation of the location of the tipping value μ_c (so that tipping occurs if $\mu < \mu_c$) of μ is harder in this case. For example, we must distinguish between a (possibly) chaotic orbit tipping and tipping with a chaotic transient. Numerical plots of μ_c (obtained using the method described earlier, with $A = 1, \eta_1 = 3, \eta_3 = 0.1$) are given in Figure 12 for the wider range of $\omega \in [0, 10]$, along with the grazing value μ_g and the large, and small, ω and estimates for μ_c. We see that μ_c agrees closely with the high-frequency estimate for values of $\omega > 3$. As ω decreases, we can see the effect of resonance, leading to a peak in the value of μ_c at $\omega \approx 1$. It is interesting that whilst the curve of the values of μ_c shows a resonant peak, the amplitude of this peak is less marked than the peak of the curve of the grazing values μ_g and occurs at a smaller value of ω. No such peak is seen in the case of the 1D map studied in [6]. The lack of smoothness of the curve around the resonance point arises from the difficulties in exactly locating μ_c remarked on above. For values of $\mu > \mu_c$, but close to μ_c in the "resonant region", we observe the complex behaviour described above arising from a period-doubling bifurcation for some μ_{pd} with $\mu_c < \mu_{pd} < \mu_g$.

https://doi.org/10.1017/S1446181125100114 Published online by Cambridge University Press

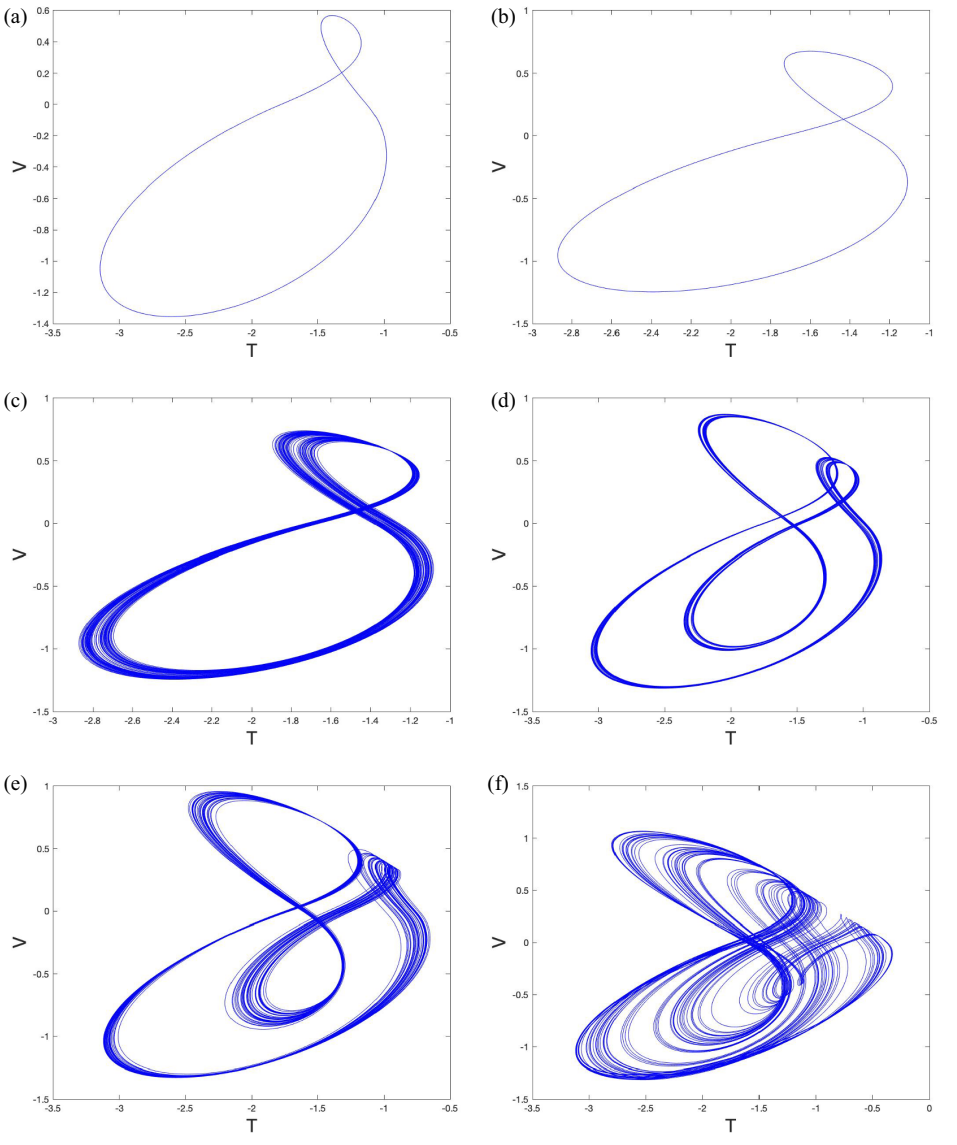

FIGURE 10. $\omega = 1$ (a–f) $\mu = 1.35, 1.29, 1.27, 1.25, 1.23, 1.21$, respectively, showing the evolution of a simple periodic orbit to a chaotic one as μ decreases.

8. Slow drift and oscillatory forcing

We now consider the case of tipping under the combination of slow drift, so that $\mu(t) = \mu_0 - \epsilon t$, $\epsilon > 0$ combined with oscillatory forcing of amplitude $A > 0$. In all cases, we start the evolution from the point $\mathbf{x}(0) = \mu_0 \mathbf{f}$ and define tipping to occur when $V = \mathbf{e}_2{}^T \mathbf{x}(t) \equiv K = 10$ with $\mu(t) \equiv \mu_{TP}$ at this point.

https://doi.org/10.1017/S1446181125100114 Published online by Cambridge University Press

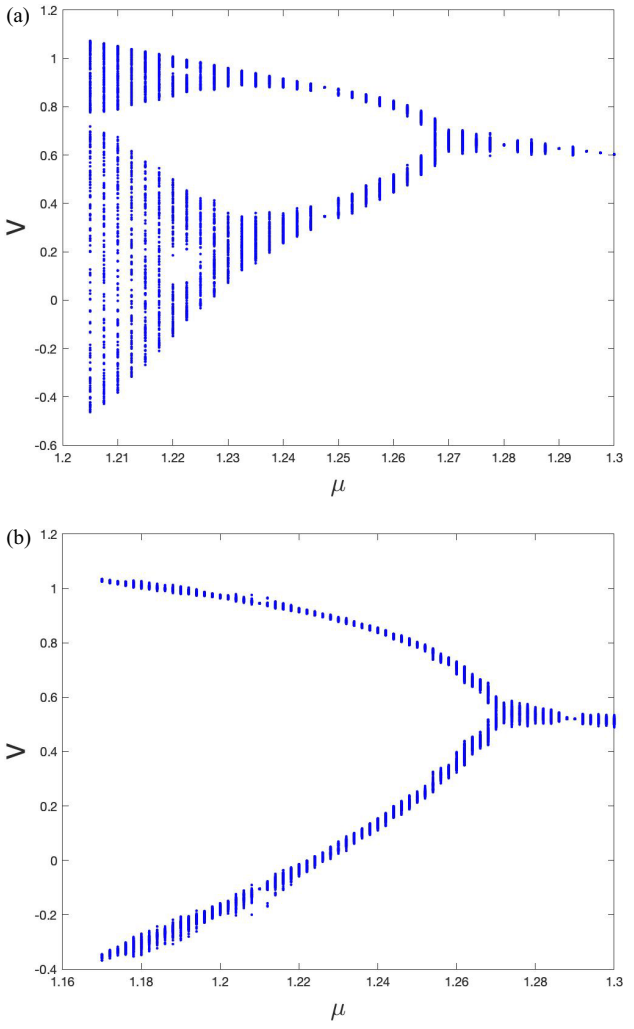

FIGURE 11. Bifurcation diagram of the *omega*-limit set of the sampled orbits as a function of μ (a) $\omega = 1$ showing the period doubling bifurcation and evolution to chaos before tipping, (b) $\omega = 1.2$ where we only see a single period-doubling bifurcation before tipping.

We consider two cases (respectively Case A and Case B). In Case A, we take $\mu_0 = 2$ so that at $t = 0$ (as can be seen from Figure 12), we have $\mu(0) > \mu_c$ for all values of ω. As t increases, we then see a transition from a stable solution to one which experiences tipping. In Case B, we consider the case of $\mu_0 = 1$. In this case, (again with reference to Figure 12), we have $\mu(0) < \mu_c$ for some values of ω, so that we immediately enter a tipping regime in this instance.

https://doi.org/10.1017/S1446181125100114 Published online by Cambridge University Press

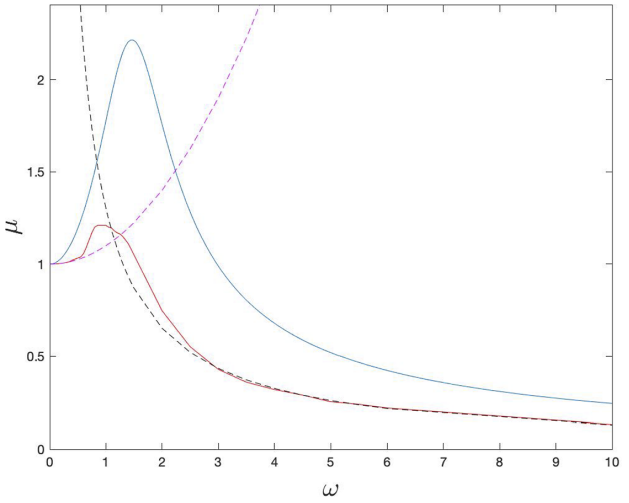

FIGURE 12. The values of the tipping point μ_c (in the case of zero drift) computed from simulations in red. These values are compared with the grazing point μ_g in blue, the high-frequency estimate $1/(\omega\lambda_c)$ for μ_c in dashed black and the low-frequency estimate $1 + 0.1\ \omega^2$ in dashed magenta. The impact of resonance is apparent in the sharp peak of the curve μ_g at $\omega \approx 1.4$ and the less pronounced peak of the curve μ_c close to $\omega = 1.4$.

Case A: $\mu_0 = 2$.

The form of tipping is presented in Figure 13(a,b) in the cases of $\epsilon = 0.1, 0.01$ and a variety of values of ω including small, large and values close to the resonant frequency of $\omega = 1.4$. We can see that the value of μ_{TP} increases in the region close to the resonant values of $\omega = 1.4$ (in a similar manner to μ_c), although this effect is combined with abrupt change in the curve (due to grazing which we describe shortly) as ω increases above one.

In Figure 14(a), we present the tipping value μ_{TP} as a function of ω for $\epsilon = 0.005, 0.01, 0.05, 0.1$. Also plotted (in red) is the location of the tipping point μ_c when $\epsilon = 0$. We note that $\mu_{TP} < \mu_c$ in all cases and that $\mu_{TP} \to \mu_c$ as $\epsilon \to 0$. We can see two things from this picture. The first is that (as expected and seen in other related systems) increasing ϵ delays tipping. Second, we see that for the smaller values of $\epsilon = 0.005, 0.01$, resonance has an impact on tipping. Observe that tipping is advanced for all of the values of $\omega \in [1, 2]$. Similar complexity is revealed when we plot the tipping value of μ as a function of the drift rate ϵ, see Figure 14(b).

For many values of ϵ and ω, particularly close to the resonant value of $\omega \approx 1.4$, we see abrupt changes in μ_{TP} as parameters vary. This makes the tipping point μ_{TP} hard to predict. For example, if $\epsilon = 0.05, 0.1$, then these jumps occur respectively if $\omega \equiv \omega_G \approx 1.2$ and $\omega \equiv \omega_G \approx 1.415$. This effect is a result of the grazing phenomena identified for the 1D system in [6] and [26], which is then enhanced by resonance. As a partial explanation of this phenomenon, we note that if $\mu(t) = \mu_0 - \epsilon t$, then there is a (unique up to terms with a decaying exponential) nonexponentially growing solution

https://doi.org/10.1017/S1446181125100114 Published online by Cambridge University Press

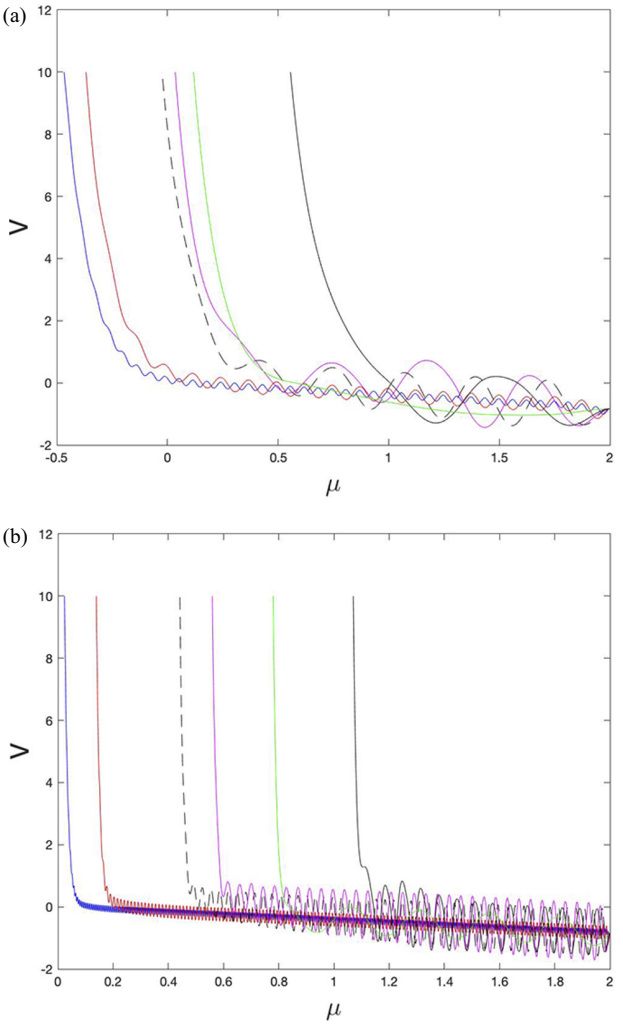

FIGURE 13. $\mu_0 = 2$. The trajectory of $V(t)$ at tipping: (a) drift $\epsilon = 0.1\omega = 10, 5, 2, 1.5, 1, 0.25$ (blue, red, black dashed, magenta, black, green); (b) drift $\epsilon = 0.01\omega = 10, 5, 2, 1.5, 1, 0.25$ (blue, red, black dashed, magenta, black, green).

in S^+ given by

$$\mathbf{x}_G(t) = \mu(t)\mathbf{s} - \epsilon(L^+)^{-1}\mathbf{s} + \mathbf{P}^+(t),$$

where the periodic orbit $\mathbf{P}^+(t)$ is given by (3.5). Suppose that ϵ is fixed. The shift in the tipping point as ω varies through ω_G arises when the orbit starting from $\mathbf{x}(0)$ grazes the orbit $\mathbf{x}_G$, so that if $\omega < \omega_G$, it stays in S^+ and tips early, or if $\omega > \omega_G$, it returns briefly to S^- and tips significantly later. The time-dependent orbits $\mathbf{x}(t)$ for ω close to

https://doi.org/10.1017/S1446181125100114 Published online by Cambridge University Press

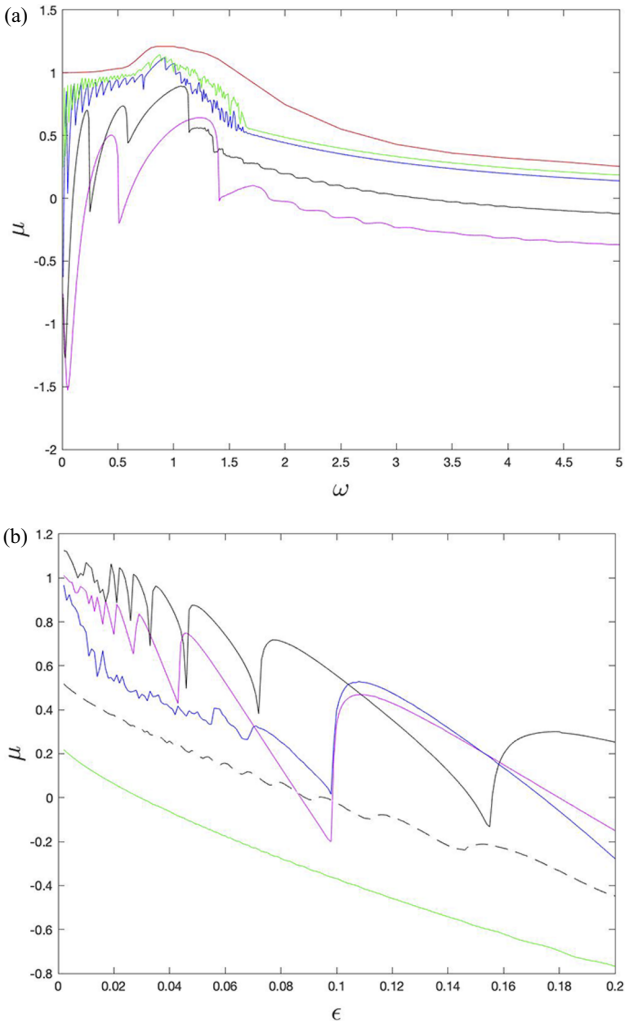

FIGURE 14. $\mu_0 = 2$. Tipping value of μ_{TP}: (a) as a function of ω with drift $\epsilon = 0.005, 0.01, 0.05, 0.1$ (green, blue, black, and magenta), showing the significant effects of resonance. Also plotted are the tipping values μ_c for $\epsilon = 0$ (red) computed earlier; (b) as a function of the drift rate ϵ when $\omega = 0.5, 1, 1.4, 2, 5$ (magenta, black, blue, dashed black, green).

ω_G are shown in Figure 15(a) and the orbits in the phase plane in Figure 15(b). Note that the red orbit has an extra "loop" briefly re-entering S^-.

Case B: $\mu_0 = 1$.

The form of tipping is presented in Figure 16(a,b) in the cases of $\epsilon = 0.1, 0.01$ and a variety of values of ω. We can immediately see from these figures that tipping is advanced for a range of forcing frequencies close to the resonant values of $\omega = 1.4$.

https://doi.org/10.1017/S1446181125100114 Published online by Cambridge University Press

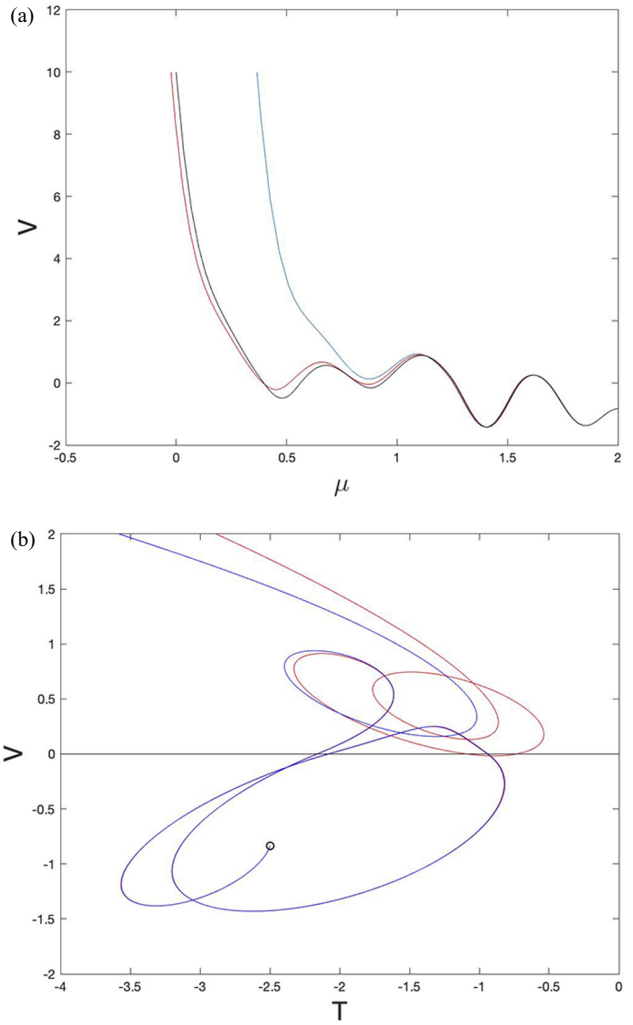

FIGURE 15. $\mu_0 = 2$, $\epsilon = 0.1$. Jumps in the tipping value μ_{TP} when $\omega = 1.4, 1.41, 1.42$ (blue, red, black) varies through ω_G: (a) variation with $\mu(t)$; (b) phase plane plotted for the cases of $\omega = 1.4$ and $\omega = 1.41$ in blue and red. These figures show the abrupt change in the tipping point close to $\omega = 1.41$ arising at a graze of the orbit with $\mathbf{x}_G(t)$. In panel (b), the blue curve tips immediately in S^+ whereas the red curve has an extra loop, briefly re-enters S^- and tips significantly later.

This is because in this case, we, in general, have $\mu < \mu_c$ so that the trajectory in this case immediately enters a tipping state. In Figure 17(a), we present the tipping point μ_{TP} as a function of ω for $\epsilon = 0.05.01, 0.05, 0.1$, together with the location of μ_c, and in Figure 17(b) the value of μ_{TP} as a function of ϵ in this case. We can see from the plot in panel (a) of the effect of ω on μ_{TP} that resonance has a bigger effect on tipping when compared with Case B. Observe that for all of the values of ω in the

https://doi.org/10.1017/S1446181125100114 Published online by Cambridge University Press

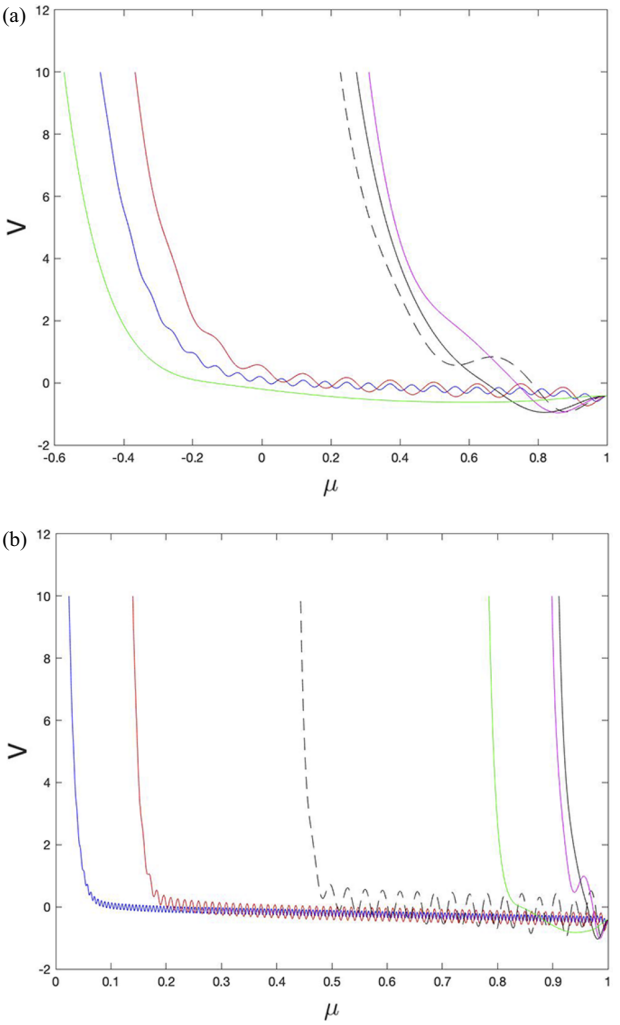

FIGURE 16. (a) $\mu_0 = 1$: drift $\epsilon = 0.1\omega = 10, 5, 2, 1.5, 1, 0.25$ (blue, red, black dashed, magenta, black, green). (b) Drift $\epsilon = 0.01\omega = 10, 5, 2, 1.5, 1, 0.25, 0.1$ (blue,red, black dashed, magenta, black, green).

"resonant region" of $\omega \in [1, 2]$ that tipping is advanced, and the range of values of ω over which the resonant affects advance is broader, and flatter, than in Case A. The curve in panel (b) is also much smoother than the related curve for $\mu_0 = 2$. It is likely that the flattening/smoothness of these curves is a consequence of taking $\mu_0 = 1$. In [6], it was shown for the 1D start with larger μ_0, that is, farther away from tipping, that the phase of the forcing plays a more significant role, which yields more fluctuations in the tipping curve as a function of ω. It is also interesting that these figures are smoother, and more monotone, than the related figures for the 1D problem for which there is no resonance.

https://doi.org/10.1017/S1446181125100114 Published online by Cambridge University Press

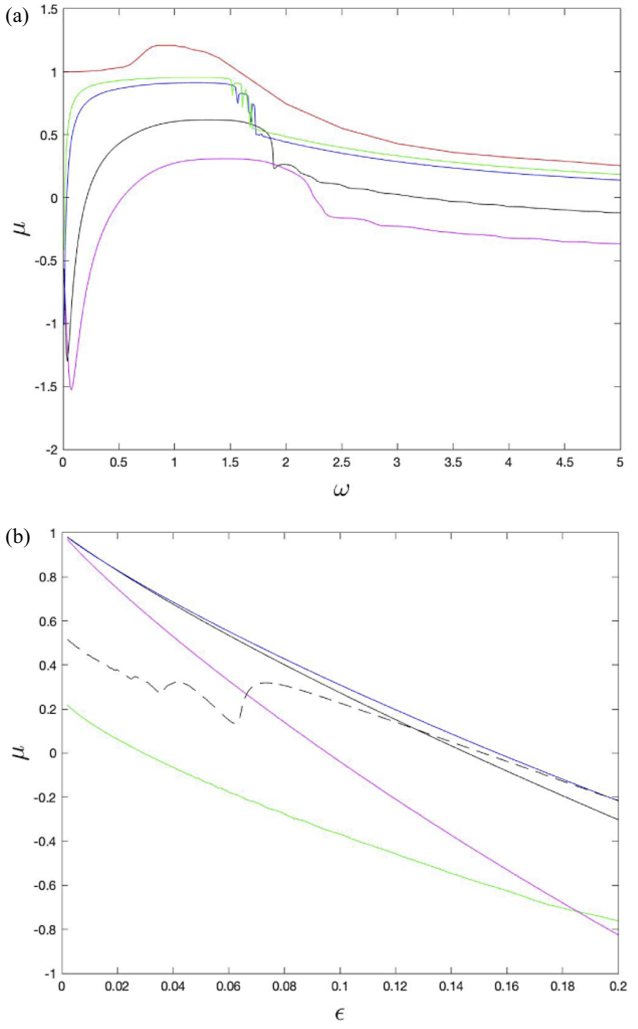

FIGURE 17. $\mu_0 = 1$: tipping value of μ_{TP} plotted (a) as a function of ω with drift $\epsilon = 0.005, 0.01, 0.05, 0.1$ (green, blue, black and magenta), showing the significant effects of resonance. Also plotted are the tipping values μ_c when $\epsilon = 0$ (red); (b) as a function of the drift rate ϵ when $\omega = 0.5, 1, 1.4, 2, 5$ (magenta, black, blue, dashed black, green).

9. Climate implications

The Stommel 2-box model we have studied is a significant simplification of the more complex models used to study tipping of the AMOC phenomenon, although it can be embedded as a part of much more complex models where tipping is observed [8, 9] and can give insights into these. In [6], a summary of the climatic implications of tipping in the simplified 1D Stommel box model is given, together with related studies of the Rooth model of thermohaline circulation (THC) [14, 20] (which is a piecewise

https://doi.org/10.1017/S1446181125100114 Published online by Cambridge University Press

smooth 3-box model with a series of switches for temperature T and salinity S). Some of these are relevant to the current study which considers the tipping dynamics close to the "off state" close to the nonsmooth fold. In particular, the first conclusion that the lack of smoothness of the system at the NSF advances tipping when the parameters are subject to slow drift. Similar results are found in [25]. These results are all similar to those discussed in this paper and the statements in these papers about very large bi-stability regions in the THC models are related to features in our study. The results in this paper also extend some of these earlier observations by including the oscillatory form of the forcing and by doing so, allow the low-dimensional models to capture variability in tipping (as discussed in [9]). The key observation (shared with the 1D model) is that oscillatory forcing terms can advance tipping (at both an NSF and at an SNB) and that oscillatory forcing combined with drift can lead to unpredictable tipping behaviour, with large changes in the tipping time as parameters (such as the drift rate and/or the forcing frequency) are varied. This has clear implications in the predictability of tipping in climate models. A significant conclusion from the study of the tipping close to the nonsmooth focus (NSF) bifurcation of the Stommel 2-box model is that the natural frequency of the focus plays an important role in tipping. In particular, if the oscillatory forcing frequency is close to resonating with this, then we see both much more complex behaviour close to tipping (such as chaotic orbits) and also significantly advanced tipping. Whilst the analysis here is only given for the 2D model, we may well expect to have an NSF embedded as a low-dimensional reduction of a bifurcation of similar nonsmooth higher dimensional problems and with various forcings of different frequencies. This then has the potential for further resonance phenomena occurring due to the existence of the focus with again complex dynamics and advanced tipping with clear climate implications. We repeat that by concentrating on the dynamics close to the NSF where we tip from the "off state" to the "on state", we have only studied a small part of the dynamics of the Stommel 2-box or more general climate models, and that the more physically relevant (to the AMOC) tipping from the "on state" is best described by the analysis for an SNB. We emphasize that comparable resonance phenomena to those seen in this paper do not appear close to tipping at a smooth SNB, and this is a novel feature of the NSF and any physical system where an NSF might occur. However, it is important to note that transitions both at the SNB and at the NSF contribute to the hysteresis window of stable behaviour seen when moving between states, for example, effecting the return to the on state in a hysteresis loop, and this impacts on the full dynamics of the climate model.

10. Conclusions and future work

We have studied the dynamics of tipping close to a nonsmooth saddle-focus (NSF) in an oscillatory forced nonsmooth system with slow drift derived from the Stommel 2-box mode. In this context, we consider the influence of both the slow variation of a critical parameter μ, and an external oscillatory forcing with amplitude A and frequency ω. Traditional studies of the detection of tipping in (for example) climate

https://doi.org/10.1017/S1446181125100114 Published online by Cambridge University Press

systems have centred around dynamic bifurcations near to the saddle-node bifurcations (SNBs), where we have real eigenvalues of the linearization with one eigenvalue becoming zero. In this setting, with slow parameter drift, it is possible to make certain estimates of the location of the tipping points close to equilibria, and these estimates vary smoothly with the parameters in the system. These estimates are typically made either by determining the system parameters, or by making measurements and observing a "slowing down" in the system response as tipping is approached and the critical eigenvalue approaches zero [9, 13]. This analysis helps to identify the lag of tipping relative to the related static SNB. Significantly, when considering a nonsmooth system close to an NSF, there is no equivalent of tipping occurring when an eigenvalue of the linearization drops to zero. Furthermore, there is a dominant effect on the dynamics of the system of the complex eigenvalues associated with the focus in the NSF, neither of which drops to zero at the bifurcation. These differences from an SNB both rule out the identification of the closeness to tipping at the NSF by monitoring the "slowing down" in the behaviour associated with a zero eigenvalue and also allow for the significant influence of resonant effects on the location of the tipping point. In future work, we plan to consider stochastic fluctuations for dynamics near the NSF in the nonautonomous Stommel model, instead of the periodic forcing considered here. In comparison with a variety of studies of noise-dominated tipping near an SNB, as in [3] and [21], our preliminary results indicate an increased sensitivity to stochastic forcing near the NSF.

In this paper, we exploit the piece-wise linear structure of the normal form reduction of the system close to the NSF of the Stommel 2-box model to give a careful analysis of the tipping behaviour close to the NSF. Observations from our results, in comparison with the SNB problem, indicate that predictions of tipping close to an NSF rely on a different balance of factors, leading to the following conclusions.

(1) The nonsmoothness of the NSF leads to more advanced and complex tipping, when compared with tipping close to the SNB. This behaviour is enhanced by the impact of resonance.
(2) The critical value of the tipping parameter μ_{TP} for the oscillatory forced system with drift close to the NSF does not behave monotonically for smaller values of ω. Indeed, we may see large transitions in the tipping times as parameters vary. This feature is also observed in SNB, for smaller ω, but its impact on tipping is enhanced by resonance. This makes the difficult problem of the estimation of tipping times in the context of noisy parameter values in these cases even more uncertain, especially if resonance is encountered.

As a broader conclusion, this analysis points to the need for care when drawing conclusions about the time and location of tipping points for systems close to an NSF, especially if we are close to resonance. Nature generally has more complexities, such as disparate time scales and multiple contributing factors, which may motivate the study of (resonant) tipping close to an NSF as a more realistic description of the behaviour of the system in certain cases than the idealized smooth models studied in the literature.

https://doi.org/10.1017/S1446181125100114 Published online by Cambridge University Press

References

[1] H. Alkhayuon, R. Tyson and S. Wieczorek, "Phase tipping: how cyclic ecosystems respond to contemporary climate", *Proc. R. Soc. A* **477** (2021) Article ID: 20210059; doi:10.1098/rspa.2021.0059.

[2] R. B. Alley, et al., "Abrupt climate change", *Science* **299** (2003) 2005–2010; doi:10.1126/science.1081056.

[3] N. Berglund and B. Gentz, "Stochastic dynamic bifurcations and excitability", in: *Stochastic methods in neuroscience* (eds. C. Laing and G. Lord) (Oxford University Press, Oxford, 2009); doi:10.1093/acprof:oso/9780199235070.003.0003.

[4] M. Bernardo, C. Budd, A. Champneys and P. Kowalczyk, *Piecewise-smooth dynamical systems: theory and applications*, Volume 163 of *Appl. Math. Sci.* (Springer Science & Business Media, Berlin, 2008).

[5] C. Budd, C. Griffth and R. Kuske, "Dynamic tipping in the non-smooth Stommel-box model, with fast oscillatory forcing", *Phys. D* **432** (2022) Article ID: 132948; doi:10.1016/j.physd.2021.

[6] C. Budd and R. Kuske, "Dynamic tipping and cyclic folds, in a one-dimensional non-smooth dynamical system linked to climate models", *Phys. D* **457** (2024) Article ID: 133949; doi:10.1016/j.physd.2023.

[7] L. Caesar, S. Rahmstorf, A. Robinson, G. Feulner and V. Saba, "Observed fingerprint of a weakening Atlantic Ocean overturning circulation", *Nature* **556** (2018) 191–196; doi:10.1038/s41586-018-0006-5.

[8] H. A. Dijkstra, *Nonlinear climate dynamics* (Cambridge University Press, Cambridge, 2013).

[9] P. Ditlevsen and S. Ditlevsen, "Warning of a forthcoming collapse of the Atlantic meridional overturning circulation", *Nat. Commun.* **14** (2023) Article ID: 4254; doi:10.1038/s41467-023-39810-w.

[10] R. Haberman, "Slowly varying jump and transition phenomena associated with algebraic bifurcation problems", *SIAM J. Appl. Math.* **37** (1979) 69–106; doi:10.1137/0137006.

[11] S. Hottovy and S. N. Stechmann, "Threshold models for rainfall and convection: deterministic versus stochastic triggers", *SIAM J. Appl. Math.* **75** (2015) 861–884; doi:10.1137/140980788.

[12] H. Kaper and H. Engler, *Mathematics and climate* (SIAM, Philadelphia, PA, 2013).

[13] T. Lenton, "Early warning of climate tipping points", *Nature Climate Change* **1** (2011) 201–209; doi:10.1038/nclimate1143.

[14] V. Lucarini and P. Stone, "Thermohaline circulation stability: a box model study. Part I: uncoupled model", *J. Climate* **18** (2015) 501–503; doi:10.1175/JCLI-3278.

[15] J. Marotzke, "Abrupt climate change and thermohaline circulation: mechanisms and predictability", *Proc. Natl. Acad. Sci. USA* **97** (2000) 1347–1350; doi:10.1073/pnas.97.4.1347.

[16] K. S. Morupisi and C. Budd, "An analysis of the periodically forced PP04 climate model, using the theory of non-smooth dynamical systems", *IMA J. Appl. Math.* **86** (2021) 76–120; doi:10.1093/imamat/hxaa039.

[17] D. Paillard and F. Parrenin, "The Antarctic ice sheet and the triggering of deglaciations", *Earth Planetary Sci. Lett.* **227** (2004) 263–271; doi:10.1016/j.epsl.2004.08.023.

[18] S. Rahmstorf, "The thermohaline ocean circulation: a system with dangerous thresholds?", *Climatic Change* **46** (2000) 247–256; doi:10.1023/A:1005648404783.

[19] S. Rahmstorf, "Ocean circulation and climate during the past 120,000 years", *Nature* **419** (2002) 207–214; doi:10.1038/nature01090.

[20] C. Rooth, "Hydrology and ocean circulation", *Prog. Oceanogr.* **11** (1982) 131–149; doi:10.1016/0079-6611(82)90006-4.

[21] J. Sieber and J. M. T. Thompson, "Nonlinear softening as a predictive precursor to climate tipping", *Philos. Trans. Roy. Soc. A* **370** (2012) 1205–1227; doi:10.1098/rsta.2011.0372(1962).

[22] D. J. Simpson, *Bifurcations in piecewise-smooth continuous systems*, Volume 70 of *World Sci. Ser. Nonlinear Sci. Ser. A Monogr. Treatises* (World Scientific, Singapore, 2010).

[23] H. Stommel, "Thermohaline convection with two stable regimes of flow", *Tellus* **13** (1061) 224–230; doi:10.3402/tellusa.v13i2.9491.

[24] J. Walsh, E. Widiasih, J. Hahn and R. McGehee, "Periodic orbits for a discontinuous vector field arising from a conceptual model of glacial cycles", *Nonlinearity* **29** (2016) Article ID: 1843; doi:10.1088/0951-7715/29/6/1843.

[25] R. Wood, J. Rodriguez, R. Smith, E. Jackson and E. Hawkins, "Observable, low-order dynamical controls on thresholds of the Atlantic meridional overturning circulation", *Clim. Dyn.* **53** (2019) 6815–6834; doi:10.1007/s00382-019-04956-1.

[26] J. Zhu, R. Kuske and T. Erneux, "Tipping points near a delayed saddle node bifurcation with periodic forcing", *SIAM J. Appl. Dyn. Syst.* **14** (2015) 2030–2068; doi:10.1137/140992229.